Supporting Information

Bergin et al. 10.1073/pnas.1500954112

SI Text

Bulk C and N Abundance Compilation and Estimation

Here we summarize the information compiled and estimated for Figs. 1 and 2 in the main text. For completeness we provide expanded versions of Figs. 1 and 2 here in Figs. S1 and S2. Table S1 provides our compilation in tabular form.

Terrestrial Worlds. The bulk silicate Earth (BSE) assumes, for simplicity, that the Earth is composed of two components: the core and the silicate mantle. In this form the BSE is the entire Earth, including its fluid envelopes (oceans and atmosphere) minus the core. Previous estimates of the C/N of the BSE differ markedly. Marty (7) estimated a C/N molar ratio of 365 ± 282, whereas in contrast Halliday's preferred model (1) amounts to 46 ± 17. This factor of 8 difference led us to revisit constraints on BSE C/N, using an approach somewhat different from previous work.

The BSE C and N inventories derive from a combination of the surface and mantle reservoirs (Table S1). For the surface reservoir, we take total carbon to be $9.3 \pm 0.9 \times 10^{22}$ gram (gm) (49) and total nitrogen to be $6.4 \pm 1.1 \times 10^{21}$ gm (50), yielding a C/N molar ratio of 16.9 ± 0.3. For the interior reservoir we consider two separate sources, based on the well-established assumption that the mantle consists of a gas-depleted source (DM) that produces midocean ridge basalts and a gas-enriched source (EM) related to oceanic island basalts (51).

We assume that the depleted reservoir constitutes between 30% and 80% of the mantle mass (52) and estimate the C concentrations of each reservoir based on C/Nb and C/Ba ratios of oceanic basalts compiled by Rosenthal et al. (53), yielding 20 ± 7 and 165 ± 55 ppm for the DM and EM, respectively.

Marty (7) and Halliday (1) estimated mantle N concentrations in part from the estimate of mantle C/N of 535 ± 224 of Marty and Zimmerman (54). However, this ratio derives from gas-liberated from basalt-crushing experiments. Because N_2 fractionates from CO_2 substantially during vesiculation, C/N ratios of basalts and their vapor bubbles vary by more than two orders of magnitude (54, 55), complicating reconstruction of source C/N. Therefore, we estimate the N concentrations of each reservoir based on N/Ar ratios. Unlike C/N, N/Ar ratios of vesicles in basalt do not change significantly owing to degassing (54, 55). The mass of Ar in the mantle is constrained by the BSE inventory of K, 280 ± 60 ppm, which over 4.55 billion years has produced $1.55 \pm 0.33 \times 10^{20}$ gm of ^{40}Ar (56). Subtracting atmospheric (57) and crustal (58) Ar masses of 6.6 and 0.9×10^{19} gm, respectively, leaves $8.00 \pm 3.3 \times 10^{19}$ gm of Ar in the present-day mantle (56). Because the N/Ar ratios of the DM and EM reservoirs are seemingly distinct (N/Ar = 74 ± 56 in DM and 105 ± 35 in EM) (59), conversion of the bulk mantle Ar mass to the bulk mantle N requires estimates of Ar concentrations in each reservoir. Taking the DM to have 3.3 ± 1.6 parts per billion (ppb) Ar [Marty and Dauphas (59), but also consistent with Allegre et al. (51) and Ballentine (60)] allows calculation of the concentration of Ar in EM by subtraction from the bulk mantle Ar reservoir. The above information is sufficient to calculate the C/N ratios of the principle terrestrial reservoirs (surface reservoir, bulk mantle, BSE) (Table S1), taking into account the uncertainties in individual concentrations and ratios must be that one accounts for the uncertainties from each constraint. This is done with a Monte Carlo simulation, as illustrated in Fig. S3, which yields C/N ratios for the bulk mantle and BSE of 80 and 46 ± 9, respectively. The mantle ratio is reported as a lognormal distribution because the arithmetic mean and SD are strongly affected by simulations that produce very small mantle N (and thus extreme C/N ratios). This BSE C/N estimate is in nearly exact agreement with the previous estimate by Halliday (1), 46 ± 17, and markedly lower than that by Marty (7).

Elemental abundances for the atmospheres of Venus and Mars are taken from the compilation of Halliday (1). The atmospheres of Mars and Venus have C/N comparable to the Earth's surface (Fig. S1), although inferences for these planets are limited by lack of constraints on interior reservoirs. In the small sample of Martian meteorites the C/N ratio appears to vary, but is elevated above the solar value (29).

Meteorites. Chondritic meteorites are a class of meteorites that escaped differentiation. Their bulk compositions generally match that of the solar photosphere, except for the most volatile elements. These meteorites are broken into groups based on their bulk chemical, mineralogical, and oxygen isotopic compositions. In addition, the proportion and sizes of the different nebular solids they contain can be used to distinguish among the groups. These groups are also categorized into three distinct classes of chondrites: the enstatite, ordinary, and carbonaceous chondrites (EC, OC, and CC, respectively). Although chondrites are thought to be aggregates of solar nebula dust, these meteorites have experienced different degrees of planetary processing in the form of thermal metamorphism and aqueous alteration. Aqueous alteration was most pervasive in the CI and CM chondrites, resulting from the melting of ice and reaction of rock with liquid water at temperatures <400–500 K. Although evidence for the action of water in other chondrites has been reported, thermal metamorphism, with meteorites reaching temperatures of up to 1,300 K, is much more common in the EC, OC, and some of the other CC (notably CV and CO) meteorites.

For meteoritic C/N ratios we have used the values determined by Alexander et al. (61, 62) for CI, CM, CR, and CO chondrites, whereas the data for CV chondrites are taken from the work of Pearson et al. (27). For these data points we have determined the weighted mean and errors based upon the individual meteoritic measurements. Thus, the error represents the range of the data relative to the errors of the individual measurements. For carbon and nitrogen elemental ratios relative to silicon we have used the bulk abundance measurements of Wasson and Kallemeyn (63), with an assumed uncertainty of 20% that is based upon their discussion of the relative uncertainties within carbonaceous chondrite groups. We also extended the error bar range based on the variation seen in the C and N content within a given class from the references above. For ordinary chondrites, information was gathered from different sources often studying the same meteorite but in different elements (24, 25, 64–66). The error reflects the range of estimated C/N ratios for each class. Abundances relative to silicon were estimated using the range of C and N from the previous sources for a given class and the average Si abundance for that class taken from Lodders and Fegley (67). For both ordinary and carbonaceous chondrites the error bars thus represent the variation of C and N rather than that of Si.

Comets. Abundances for comet Halley rely on compilations/analysis of Fomenkova (68), Jessberger (69), Delsemme (70), and Wyckoff et al. (15). In situ analysis of the refractory carbonaceous component was performed by instruments on board Vega-1, Vega-2, and Giotto spacecraft that performed fly-bys within the coma and that, with further analysis, provided elemental

abundances. For carbon, nitrogen, and silicon, Fomenkova (68) states that gas and dust abundances of Halley for carbon are solar, nitrogen is a factor of 2 below solar, and silicon is within a factor of 2 of solar. Jessberger (69) states that the rock-forming elements are within a factor of 2 of solar and chondritic; thus we adopt a factor of 2 error on the Si abundance, which then dominates that calculation. For carbon we assume that 36% is bound in molecular volatiles (70), whereas only 10% of the nitrogen inventory is tied up in such species (15). Assuming solar abundances the C/N (gas and dust) ratio is $(C/N)_{\odot}/2$ and we adopt a 50% error. The evaporation of Sun-grazing comets provides another unique estimate of bulk cometary abundances. Two comets have measurements of C and Si (C-2003K7 and C/2011 W3:Lovejoy) (71, 72), whereas Comet Lovejoy has an additional measurement of nitrogen (provided by J. Raymond and given here). Errors are assigned a value of 50% that is based upon the estimated range in the C/Si ratio for C-2003K7 (71) and we extend this to the other measurements.

Regarding the formation zone of Halley and the Sun-grazing comets, we note that the two Sun-grazing comets could be fragments of the same progenitor (73). However, it is likely that the larger parent(s) originated within the Oort cloud (74), which itself is populated from comets formed near the giant planets and perturbed to larger orbits (75). The origin of Halley-type comets has been a matter of debate; however, the recent detection of a trans-Neptunian object in a highly inclined retrograde orbit suggests a source region for Halley-type comets with a primordial origin at large distances (>50 AU) (76).

Interstellar Medium. In the ISM, elemental abundance measurements can be obtained via spectroscopic techniques toward low-density (<1,000 cm^{-3}) atomic gas in front of bright stars. These gas-phase data are compared with some reference abundance measurements, either the Sun or young stars (which likely represent the original composition of gas in their galactic location). For a given element the deficit in abundance from the gas compared with the solar/stellar standard is assumed to be sequestered into dust grains. The presence of dust along these lines of sight is confirmed by its differential absorption effects on the broad-band stellar spectrum.

Thus, Jensen et al. (77) surveyed 30 sight lines in transitions of atomic nitrogen and compiled abundances from previous work. They find a gas phase nitrogen abundance at high extinction ($A_V > 1^m$) of 49 ± 4 ppm (relative to H) and, using adopting B stars as the standard, find that 14 ppm is missing from the gas phase. This missing nitrogen could potentially be incorporated into the carbonaceous dust component and represents our limit for nitrogen in the solid state.

Based on elemental abundances measured toward sight lines that intersect diffuse interstellar gas/dust, the wavelength-dependent extinction of starlight, and spectral features with unidentified carriers (e.g., the 2,200-Å extinction bump and mid-IR emission bands), it is thought that a significant percentage of interstellar carbon resides in some refractory component. In five sight lines with high average density ($\log_{10}\langle n_H/cm^{-3}\rangle > 0.5$), Parvathi et al. (78) estimate that 371 ± 37 ppm (relative to H) of carbon reside in interstellar dust grains, assuming B-star standard abundances. Along the same, higher-density sight lines the abundance of gas-phase carbon is 94 ± 13 ppm. The recent dust models of Jones et al. (12) and Chiar et al. (13) adopt 233 ppm and 150 ppm, respectively. For our purposes it is clear that there is a large amount of carbon in interstellar dust grains and we adopt 250 ± 50 ppm to account for the disparate abundance estimates.

As noted in the main text the median value of C/N ratio of interstellar ices is ∼12 (14). These measurements do not account for N or N_2, which are infrared inactive. Based on the similar sublimation temperature between CO and N_2 (79), we assume $(CO/N_2)_{ice} \sim 1$. Further, assuming all N is in N_2 and 50% of C is in CO gives a C/N ratio for ices of ∼1.8.

Assumptions for Equilibrium Calculations

In our calculations in Fig. 4 we made the following assumptions. For oxidized, $D_C^{met/sil} = 500$; $D_N^{met/sil} = 20$; C in vapor is assumed to be chiefly CO_2, with depth-averaged C solubility in silicate liquid of 1.6 ppm/MPa (40); and N is dissolved as N_2, with depth-averaged solubility = 1 ppm/MPa (41). For reduced, $D_C^{met/sil} = 1{,}000$; $D_N^{met/sil} = 20$; C in vapor is assumed to be chiefly CO, with solubility equal to 1 ppm CO/MPa (47); and N is dissolved as N_2, with solubility = 1 ppm/MPa (41). For very reduced, $D_C^{met/sil} = 1{,}000$, $D_N^{met/sil} = 20$, C is highly insoluble (0.05 ppm/MPa), and N is highly soluble (50 ppm/MPa). We note that quantitative solubilities for the third case in Fig. 4 lack constraints; for C and N they must be very low and high, respectively.

Kinetic Chemical Model

Lodders (80) explored the chemistry in the solar system within the framework of the 50% condensation temperature for thermodynamic equilibrium. This concept implies that the chemical species produced in the disk are independent of the starting materials. However, as discussed by Lodders, the history and carriers matter for reactive volatile elements. Thus, the 50% condensation temperature is not a useful guide in this case, as thermodynamic equilibrium will not be achieved and we adopt a kinetic model to explore the evolution of these elements.

The kinetic chemical model presented in Fig. 3 of the main text is a compilation of chemical abundance predictions from the model of Cleeves et al. (81). The physical structure is a 2D azimuthally symmetric model that is motivated by the observations of solar analog protoplanetary disks. Greater details regarding the exact physical prescription can be found in the references listed above. For completeness the basic physical structure is provided in Fig. S4. Our methodology is to take an adopted dust density structure constrained by observations. The gas density in this model, compared with the dust, has a vertically integrated gas to dust mass ratio of 100. However, in practice the gas to dust mass ratio is higher in the upper layers and reduced in the midplane to mimic the effects of dust settling. With the gas and dust density prescribed we determine the dust temperature structure, using the radiative equilibrium code TORUS (82). For this calculation the central star is assumed to have mass of $M = 1.06\ M_{\odot}$, $R = 1.83\ R_{\odot}$, and an effective temperature of 4,300 K. Due to high densities and frequent dust–gas collisions, the gas temperature is coupled to the dust for much of the disk mass, but is elevated at the surface due to stellar X-ray heating. Within the framework provided by the dust and gas density we determine the UV and X-ray photon fields. For the input spectra in the UV we use the spectrum measured toward TW Hya, the closest star/disk system. The X-ray spectrum is estimated assuming a two-temperature optically thin plasma, with one component at T =9 MK and another at 30 MK, and propagated assuming X-ray photoabsorption cross-sections. The resulting distribution of UV and X-ray flux is then calculated using the Monte Carlo model developed by Bethell and Bergin (83). For more explicit details and complete references the reader is referred to Cleeves et al. (81).

The chemical model includes gas-phase processes, gas–grain interactions, and a limited set of grain surface reactions for the main carriers of C, O, and N linked through a network of ∼5,900 reactions, assuming initial chemical abundances (81). To create Fig. 3 we ran the model for 1 My and compiled the predicted abundances. Based on these predictions we summed up the abundances of all carriers of carbon and nitrogen to isolate the main carriers. These are (both gas and ice phase): CO, CO_2, N_2, NH_3, and organics. Refractory carbon contains ∼50% of elemental carbon in the interstellar medium and we assume it is oxidized (19) interior to ∼2 AU where it is released as CO (listed as CO′ in Fig. 3). The location in the disk where this process is

active is highly uncertain. The main organic carriers of C, where the abundances were summed for Fig. 3 (separately as gas and ice), are HC_3N, C_3, HCN, CH_3OH, C_3H, HNC, C_4H_2, C_2H_4, OCN, C_3O, H_2CO, and CH_4; for nitrogen the organic carriers are HC_3N, HCN, HNC, and H_2CN. An important issue is the presence of NH_3 in the ices even at 2 AU. This is due to the relatively high sublimation temperature of NH_3 compared with N or N_2 (at relevant pressures, $NH_3 \sim 80$ K for pure ice or higher if bound with water; $N_2 \sim 20$ K) (79, 84). In this light the depletion of nitrogen in cometary ices is difficult to interpret. However, a recent exploration of nitrogen in protoplanetary disks can match the nitrogen content in cometary ices provided nitrogen is initially supplied to the disk as atomic N, which is then converted to gaseous N_2 (85).

The estimated sublimation temperature of organic ices depends on the binding strength to the surface; based on laboratory measurements (86), this is on the order of 150–250 K for low molecular weight species (the latter corresponds to a binding energy of 7,500 K, for a molecular mass of 60 atomic mass units and a pressure of $\sim 10^{-4}$ bar). For carbon in organic "refractory" form we can use the literature on sublimation enthalpies for hydrocarbons that are $\sim$ 100 kJ/mol (87), with a corresponding sublimation temperature of $\sim$ 400 K. Some fraction of the C may be present as macromolecular, cross-linked species and would survive to even higher temperatures.

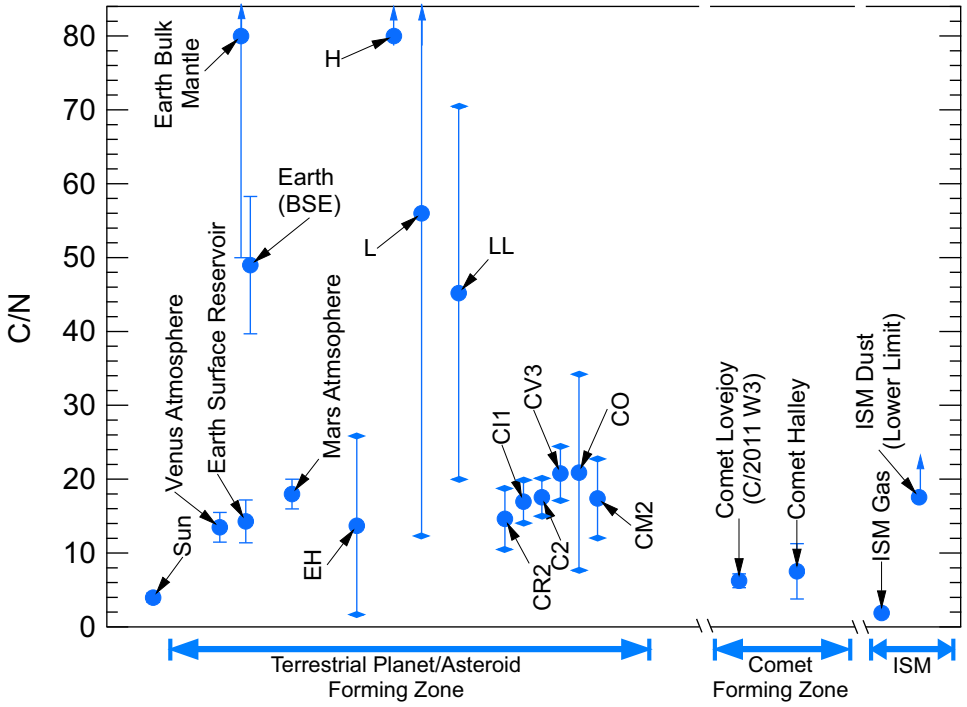

Fig. S1. Expanded version of Fig. 1 in the main text. Shown is the ratio of bulk (or as noted) carbon relative to nitrogen in various solar system bodies and ISM. Errors denoted with a diamond represent ranges within the samples and not the measurement error. Normal error bars represent the 1σ uncertainty in the measurement.

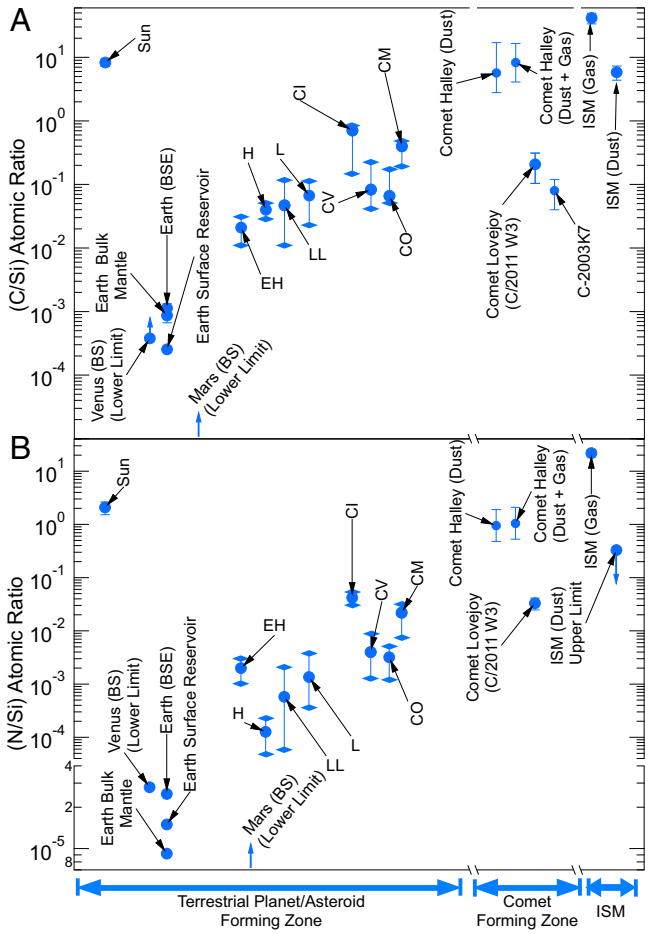

Fig. S2. Expanded version of Fig. 2 in the main text. Shown are (*A*) bulk elemental carbon to silicon atomic ratio and (*B*) nitrogen to silicon atomic ratio. Errors denoted with a diamond represent ranges within the samples and not the measurement error. Normal error bars represent the 1σ uncertainty in the measurement.

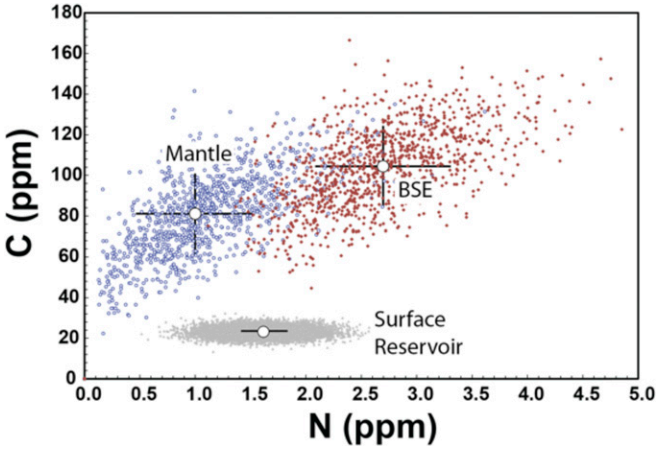

Fig. S3. Results of Monte Carlo simulation showing compositions of surface reservoir, bulk mantle, and bulk silicate Earth (BSE). Concentrations are in parts per million by weight, calculated from the mass of C and N in each reservoir divided by the mass of the BSE (4×10^{27} gm). The Monte Carlo simulation was performed with 1,000 individual calculations.

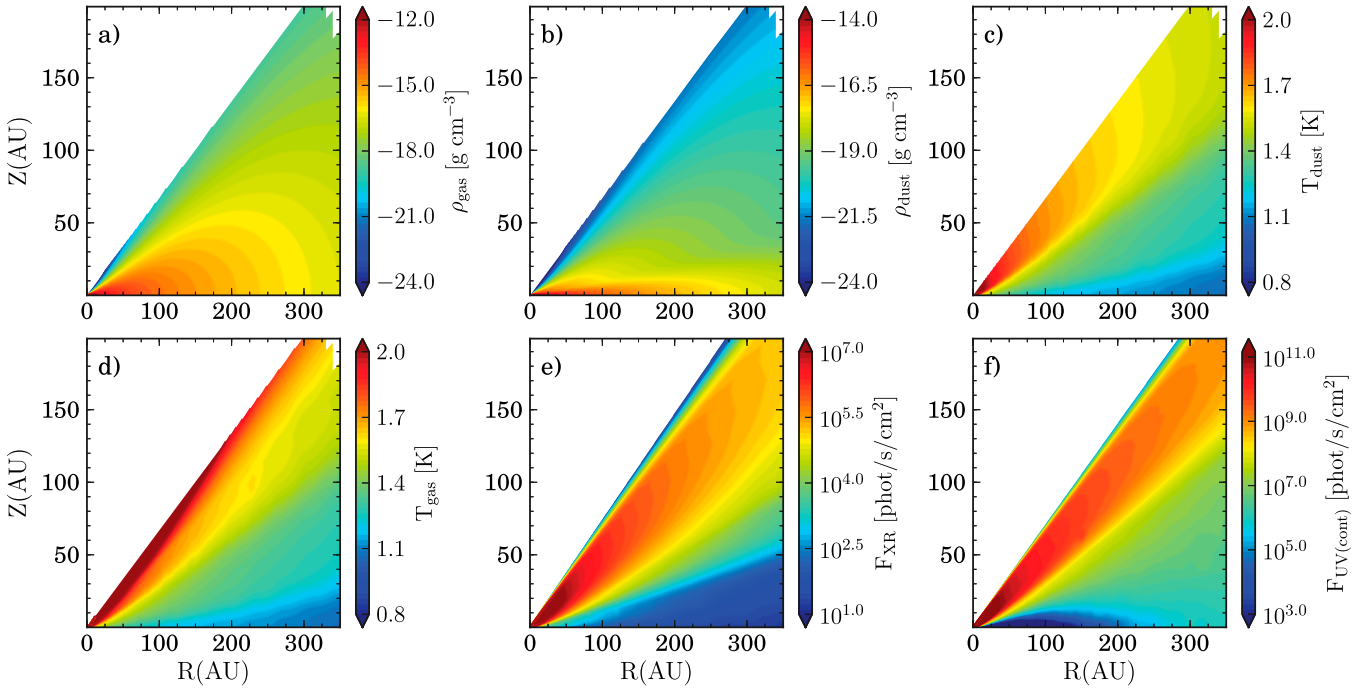

Fig. S4. Illustration of the adopted disk physical structure for the kinetic model as a function of radius (R) and height (Z). This includes the gas density (*A*), dust density (*B*), dust temperature (*C*), gas temperature (*D*), UV photon flux (*E*), and X-ray photon flux (*F*). Reprinted with permission from ref. 81.

Table S1. Compilation of C and N content in solar system bodies

Source	Relative atomic ratio* C/Si	N/Si	C/N	Notes on C/N ratio
Terrestrial planets				
Earth, BSE	$1.1(-3)^{+2.0(-4)}_{-2.0(-4)}$	$2.5(-5)^{+5.0(-6)}_{-5.0(-6)}$	49.0 ± 9.3	This study[†]
Earth surface	$2.5(-4)^{+2.2(-5)}_{-2.2(-5)}$	$1.5(-5)^{+2.7(-6)}_{-2.7(-6)}$	14.3 ± 2.9	This study[†]
Earth mantle	$8.7(-4)^{+2.2(-4)}_{-2.2(-4)}$	$9.2(-6)^{+4.6(-6)}_{-4.6(-6)}$	80 ± 35	This study[†]
Venus atmosphere	$3.8(-4)$	$2.8(-5)$	13.5 ± 2	(1)[†]
Mars atmosphere	$1.6(-7)$	$8.8(-9)$	18.0 ± 2	(1)[†]
Meteorites[‡]				
CI	$0.71^{+0.14}_{-0.50}$	$0.042^{+0.011}_{-0.011}$	17.0 ± 3.0	CI1 (61)
CO	$0.07^{+0.11}_{-0.02}$	$0.003^{+0.002}_{-0.002}$	12.2 ± 3.2	CO3 (62)
CM	$0.40^{+0.08}_{-0.21}$	$0.022^{+0.010}_{-0.015}$	21.7 ± 1.3	CM2 (61)
CV	$0.08^{+0.14}_{-0.04}$	$0.004^{+0.005}_{-0.003}$	20.8 ± 3.7	CV3 (27)
L	$0.07^{+0.04}_{-0.04}$	$0.001^{+0.002}_{-0.001}$	45.2 ± 25.2	L3 (24, 25, 65, 66)
LL	$0.07^{+0.04}_{-0.04}$	$0.001^{+0.002}_{-0.001}$	56.0 ± 43.7	LL3,5 (24, 25, 65)
H	$0.04^{+0.01}_{-0.01}$	$0.00013^{+0.0001}_{-0.00008}$	452.0 ± 298.0	H3,4 (24, 64, 66)
EH	$0.022^{+0.008}_{-0.008}$	$0.002^{+0.001}_{-0.001}$	13.7 ± 12.1	EH5,6 (29)
Comets				
Comet Halley, dust	$5.7^{+11.4}_{-2.9}$	$1.0^{+1.0}_{-0.5}$	—	(15, 68, 70)
Comet Halley, dust + gas	$8.3^{+8.3}_{-4.2}$	$1.1^{+2.1}_{-0.5}$	7.5 ± 3.75[§]	(68)
Comet C/2011 W3	$0.21^{+0.10}_{-0.10}$	$0.03^{+0.01}_{-0.01}$	6.2 ± 0.9	(72)[¶]
Comet C/2003 K7	$0.08^{+0.04}_{-0.04}$	—	—	(72)
Interstellar medium				
ISM, gas	$41.7^{+8.0}_{-8.0}$	$21.9^{+3.4}_{-3.4}$	1.9 ± 0.3	(77, 78)
ISM, dust	$5.85^{+1.5}_{-1.5}$	< 0.33	> 17.57	(12, 13, 77, 78)

*See text for discussion of the upper and lower bounds, which represent ranges in measurements and/or uncertainties in a compiled measurement.
[†]$1.0(-4)$ corresponds to 1.0×10^{-4}.
[‡]As noted in the discussion regarding meteorites, the C/N ratio in carbonaceous chondrites was determined from different references from the C/Si and N/Si ratios. However, the measurements are consistent with the given upper and lower bounds.
[§]For Comet Halley the errors on the C/Si and N/Si ratios are dominated by our assumed factor of 2 error on the Si measurement. For the C/N ratio we assume a 50% error.
[¶]Nitrogen abundances relative to Si and C/N ratio provided by J. Raymond and given here.